Ahr-Foxp3-RORγt Axis Controls Gut Homing of CD4+ T Cells by Regulating GPR15

Lifeng Xiong[1], **Joseph W. Dean**[1], **Zheng Fu**[1], **Kristen N. Oliff**[1], **John W. Bostick**[1], **Jian Ye**[1], **Zongming E. Chen**[2], **Marcus Mühlbauer**[3], **Liang Zhou**[1,*]

[1]Department of Infectious Diseases and Immunology, College of Veterinary Medicine, University of Florida, Gainesville, FL 32608, USA

[2]Department of Laboratory Medicine and Pathology, Mayo Clinic, Rochester, MN 55905, USA

[3]Division of Gastroenterology, Hepatology and Nutrition, College of Medicine, University of Florida, Gainesville, FL 32608, USA

Abstract

The orphan chemoattractant receptor GPR15 is important for homing T lymphocytes to the large intestine, thereby maintaining intestinal immune homeostasis. However, the molecular mechanisms underlying the regulation of GPR15 expression remain elusive. Here we show a central role of the aryl hydrocarbon receptor (Ahr) in promoting GPR15 expression both in mice and human, thus gut homing of T lymphocytes. Mechanistically, Ahr directly binds to open chromatin regions of the *Gpr15* locus to enhance its expression. Ahr transcriptional activity in directing GPR15 expression was modulated by two transcription factors, Foxp3 and RORγt, both of which are expressed preferentially by gut Tregs *in vivo*. Specifically, Foxp3 interacted with Ahr and enhanced Ahr DNA binding at the *Gpr15* locus, thereby promoting GPR15 expression. In contrast, RORγt plays an inhibitory role at least in part by competing with Ahr binding to the *Gpr15* locus. Our findings thus demonstrate a key role for Ahr in regulating Treg intestinal homing under the steady state and during inflammation, and the importance of Ahr-RORγt-Foxp3 axis in regulating gut homing receptor GPR15 expression by lymphocytes.

One Sentence Summary

GPR15 expression is promoted by Ahr in an evolutionarily conserved manner via cooperation with Foxp3, but inhibited by RORγt.

*Correspondence: Liang Zhou; Tel: 352-294-8293; Fax: 352-392-9704; liangzhou497@ufl.edu.

Introduction

GPR15, an orphan guanine nucleotide-binding protein (G protein)-coupled chemo-attractant receptor (GPCR), was originally discovered based on its similarity to other members of the GPCR family (1) and is also known as the HIV or the simian immunodeficiency virus co-receptor (2). It has recently been demonstrated that GPR15 is critical for intestinal homing of both regulatory T (Tregs) and effector T cells (Teffs) in mice and in human, suggesting a physiological role for this receptor in regulating intestinal tissue immune homeostasis (3, 4). A natural GPR15 endogenous ligand was also identified in human and mouse epithelial tissues that are exposed to the environment, including the colon and skin (5). GPR15 is reported to be important for the migration of dendritic epidermal T cells (DETCs) to the skin in early postnatal murine development (6) but seems to be dispensable for the pathogenesis of murine psoriasiform dermatitis (7).

Human Tregs, especially those in the large intestine, were shown to express higher levels of GPR15 than Tregs in other tissues (3). However, it has also been reported that human T helper (Th) 2 cells but not Tregs express GPR15 (4). It was shown that GATA3 and Foxp3 bind to a *Gpr15* enhancer, leading to a model that GATA3 promotes and Foxp3 suppresses GPR15 expression in human Th2 cells and Tregs, respectively (4). It is known that Foxp3 can function as a transcriptional repressor (8, 9). Compared with human Tregs, reduced Foxp3 binding at a downstream *Gpr15* enhancer site in murine Tregs was speculated to account for expression of GPR15 due to less inhibition by Foxp3 (4). However, this notion of Foxp3 inhibition requires the support of functional evidence in both human and mouse Tregs. In addition, it is largely unknown if Foxp3 and other factor(s) work together to regulate *Gpr15* transcription in mouse Tregs.

The aryl hydrocarbon receptor (Ahr) is an environmental sensor that can detect xenobiotic ligands like environmental toxins (e.g., dioxin) as well as endogenous ligands generated from host cells, microbiota, and diet (e.g., tryptophan metabolites) (10–13). Our previous findings indicate that there is higher expression of Ahr by gut Tregs compared with Tregs in other anatomic locations, representing a potential tissue adaptation of the host that can be used to respond readily to ligands in the gut (14). Intriguingly, the reduction of *Gpr15* mRNA in Ahr-deficient Tregs isolated from the large intestine suggests a potential role for Ahr in the regulation of GPR15 expression and Treg gut homing (14). In this study, we show that GPR15 expression is controlled by the environmental sensor Ahr in all CD4$^+$ T helper cell subsets but not CD8$^+$ T cells in the gut, highlighting an environmental effect on GPR15 expression. We further show that *Gpr15* is among the top-ranked Ahr direct-binding target genes in Tregs and Th17 cells. Mechanistically, Ahr cooperates with Foxp3 to enhance GPR15 expression in Tregs. In contrast, RORγt antagonizes Ahr DNA binding to the *Gpr15* locus in both Tregs and Th17 cells, thus inhibiting GPR15 expression. These data suggest that an intricate Ahr-Foxp3-RORγt axis controls GPR15 expression in CD4$^+$ T cells to regulate their gut homing.

Results

Ahr-dependent GPR15 is most prominently expressed by large intestine Tregs

To determine the GPR15 expression among various murine T cells, GPR15 protein was measured by fluorescence-activated cell sorting (FACS) staining in Th1, Th2, Th17, Treg, as well as CD8$^+$ T cells. Compared with other cell subsets, Tregs expressed the highest level of GPR15 protein (Fig. 1, A and B). In addition, GPR15 expression by Tregs in the large intestine (LI) was higher than that in the small intestine (SI) or in the spleen (Sp) (Fig. 1, A and B, and fig. S1, A and B), consistent with previous report that GPR15 was preferentially expressed by large intestinal Tregs, indicated by GFP signals using $Gpr15^{gfp/+}$ reporter mice (3).

No differences in expression were observed in CD8$^+$ T cells from the large intestine of $Ahr^{-/-}$ mice relative to littermate control $Ahr^{+/+}$ mice, but GPR15 expression in all CD4$^+$ T cell subsets, including Th1, Th2, Th17 and Tregs, was decreased in the large intestine of $Ahr^{-/-}$ mice compared with littermate controls (Fig. 1, A and B). Of note, Ahr was largely dispensable for the expression of GPR15 in the splenic or small intestinal T cells, except for small intestinal Tregs (fig. S1, A and B), underscoring a key role of Ahr regulating GPR15 expression by gut Tregs. To determine the cell-intrinsic function of Ahr, we further examined GPR15 expression in $Ahr^{f/-}Foxp3^{Yfp-Cre}$ mice, which have specific deletion of Ahr in Tregs (14). Consistent with the data of $Ahr^{-/-}$ mice, ablation of Ahr in Tregs markedly reduced GPR15 expression in the intestinal Tregs (Fig. 1, C and D).

We next sought to determine the consequences of Ahr activation on GPR15 expression *in vivo*. Activation of Ahr in $Ahr^{dCAIR/+}$ mice, in which constitutively active (CA-Ahr) is expressed from the endogenous *Ahr* locus in all cells (14), enhanced GPR15 expression in CD4$^+$ T cells but not in CD8$^+$ T cells (Fig. 1, E and F, and fig. S1, C and D). $Ahr^{CAIR/+}Foxp3^{Yfp-Cre}$ mice have Foxp3$^+$ T cell-specific expression of CA-Ahr and had significantly higher GPR15 expression in Tregs compared with $Ahr^{+/+}Foxp3^{Yfp-Cre}$ mice (Fig. 1, G and H, and fig. S1, E and F). Analysis of GPR15 expression indicated that Ahr enhanced GPR15 expression in a dose-dependent manner in gut Tregs in $Ahr^{CAIR/+}Foxp3^{Yfp-Cre}$ mice (Fig. 1, I to K). We further determined the mRNA level of *Gpr15* in Th1, Th2, Th17, CD8, or Treg cells sorted from the large intestine of Ahr-deficient, Ahr-sufficient or Ahr constitutively active mice. Consistent with the positive association of GPR15 protein expression with Ahr in gut CD4$^+$ T helper cells, *Gpr15* mRNA was regulated by Ahr in a dose-dependent manner, similar to the Ahr prototypical target gene, *Ahrr* (Ahr repressor), (fig. S1, G and H).

Ahr is a sensor whose activity can be modulated by environmental stimuli (11, 12), so we evaluated the effect of dietary Ahr ligand on GPR15 expression. We fed C57BL/6 wild-type mice with a previously reported Ahr-ligand-deficient diet (AIN-76A) with or without the addition of Ahr ligand, indole-3-carbinol (I3C) ("76A" or "76A + I3C") (15). Depletion of Ahr ligand from diet reduced GPR15 expression (compare Fig. 1, A and L), while addition of Ahr ligand I3C, markedly enhanced GPR15 expression in intestinal CD4$^+$ T cell subsets (Fig. 1L, and fig. S2, A to C). In contrast, dietary ligand manipulation had no effect on GPR15 expression in gut CD8$^+$ T cells, consistent with a dispensable role for Ahr. A similar

dietary modification in $Ahr^{f/-}Foxp3^{Yfp-Cre}$ mice confirmed the cell intrinsic regulation of GPR15 expression by Ahr, and specific deletion of Ahr in Tregs abrogated the effect of Ahr ligand (I3C) diet to promote GPR15 expression in Tregs, but not in other CD4+ subsets (fig. S2D). Together, these data demonstrate that Ahr is a positive regulator of GPR15 expression in CD4+ T cells.

Gpr15 is a direct target gene of Ahr in Tregs and Th17 cells

Emerging evidence indicates that Ahr, a ligand-dependent transcription factor, plays a crucial physiological role in various lymphocytes (16, 17). However, our understanding is incomplete given the absence of genome-wide analysis of endogenous Ahr binding in CD4+ T cells. As an initial step, we performed chromatin immunoprecipitation sequencing (ChIP-seq) of Ahr using *in vitro* differentiated Tregs (iTregs) and Th17 cells. By ranking Ahr binding intensity at high-confidence regions from ChiP-seq data, analysis indicated that Ahr-binding peak ranked #6 among 16,298 Ahr-binding peaks in iTregs and #7 among 24,368 Ahr-binding peaks in Th17 cells, respectively. Of note, *Gpr15* gene is among the top genome-wide targets of Ahr, together with *Cyp1a1* (cytochrome P450 1A1), *Cyp1b1* (cytochrome P450 1B1) and *Ahrr* (Ahr repressor), which are prototypical Ahr target genes (11, 18), in both iTregs and Th17 cells (Fig. 2, A and B). These data suggest a key function of Ahr as a transcription factor to regulate GPR15 expression in Tregs and Th17 cells.

To delineate the molecular regulatory mode of Ahr, we assessed Ahr binding at the *Gpr15* locus and revealed two significant binding peaks (at +15 kb and +17 kb from the transcription start site) (Fig. 2C). The recruitment of Ahr to these sites was corroborated by ChIP-qPCR of Ahr (Fig. 2, D and E). Intriguingly, these Ahr binding peaks coincided with the transposase-accessible chromatin sequencing (ATAC-seq) peaks that we previously identified in large intestinal Tregs (Fig. 2C and ref. (14)), suggesting a relationship between Ahr DNA binding and chromatin accessibility (Fig. 2C). Although somewhat reduced without statistical significance, chromatin accessibility at +15 kb or +17 kb site was largely unchanged in Ahr-deficient Tregs (Fig. 2C), indicating that chromatin opening at these loci are molecular events that precede the Ahr DNA binding.

To further determine the functional relevance of Ahr DNA binding in regulation of GPR15, we transduced naïve CD4+ T cells from $Ahr^{-/-}$ mice with a retroviral construct encoding wild-type Ahr or its DNA-binding mutant (Ahr Y9A: Tyr to Ala point mutation at 9th amino acid) (19), and then differentiated them into iTregs. Whereas wild-type Ahr restored GPR15 expression to a level comparable to that of iTregs differentiated from naïve T cells of WT ($Ahr^{+/+}$) mice, DNA-binding mutant (Ahr Y9A) abolished the ability of Ahr to promote GPR15 expression (Fig. 2, F and G). Collectively, our data demonstrate that Ahr controls GPR15 expression via direct binding to the *Gpr15* locus.

Foxp3 cooperates with Ahr to positively regulate GPR15 expression

Given that Tregs expressed the highest amount of GPR15 compared to other T cell subsets, we next determined the regulatory effect of Foxp3 on GPR15 expression. We knocked down the expression of Foxp3 by using a Foxp3-specific short hairpin RNA (shRNA) vector (shRNA:Foxp3, LMP1066) in CD4+ T cells differentiated under iTreg-polarizing condition

with or without Ahr ligand 6-Formylindolo[3,2-b]carbazole (FICZ) addition (fig. S3A and ref. (20)). GPR15 protein expression was significantly reduced by LMP1066, but not by control hairpin vector LMP (shRNA:EV) or an shRNA targeting CD8 gene (shRNA:CD8) (21) (Fig. 3, A and B), suggesting a positive role for Foxp3 to promote GPR15 expression. Forced expression of Foxp3 significantly elevated GPR15 expression in iTregs from $Ahr^{+/+}$ mice but not from $Ahr^{-/-}$ mice (Fig. 3, C and D). Notably, Foxp3 FKH, a mutant that lacks DNA-binding Forkhead domain (FKH), inhibited Foxp3-driven GITR (glucocorticoid-induced TNFR family related gene) expression but had a similar effect promoting GPR15 expression as wild-type Foxp3 (Fig. 3, C and D, and fig. S3B). Furthermore, co-transduction of retroviral constructs expressing Ahr and wild-type Foxp3 or Foxp3 FKH in sorted naïve CD4$^+$ T cells cultured under Th0 condition cooperatively enhanced GPR15 expression, whereas Foxp3 transduction alone did not affect GPR15 expression (Fig. 3, E and F, and fig. S3C). In addition, co-transfection of Foxp3 with Ahr increased the luciferase reporter activity driven by the $Gpr15$ promoter (1400 bp) plus the enhancer (+15 kb to +17 kb) that contained the Ahr binding sites. The cooperative effect of Foxp3 and Ahr was also evident in the presence of Ahr ligands (FICZ and indole-3-aldehyde (I3A)) (fig. S3D and E). Together, these data suggest that the Foxp3-promoted GPR15 expression is dependent on Ahr but not Foxp3 DNA binding activity.

By analyzing the previously published ChIP-seq data (22), Foxp3 binding was detected at the open chromatin regions at the $Gpr15$ locus in Tregs (+17 kb and + 15 kb) (Fig. 2C). Consistent with this, we observed binding of Foxp3 at these regions of $Gpr15$ locus in iTregs by ChIP-qPCR (Fig. 3G). Notably, the binding of Foxp3 at the $Gpr15$ locus in Ahr-deficient iTregs was similar to wild-type iTregs, whereas the recruitment of Ahr to the $Gpr15$ locus was reduced upon knocking down Foxp3 in iTregs (Fig. 3H). These data support a concerted action between Ahr and Foxp3 to promote GPR15 expression.

To further determine the molecular mechanism underlying the cooperativity, we performed a co-immunoprecipitation assay between Ahr and Foxp3, and their mutants respectively (fig. S3, F to I). An interaction was observed between Ahr and Foxp3 (fig. S3, F to I), and either the Per-Arnt-Sim (PAS) or basic Helix-Loop-Helix (bHLH) domain of Ahr is necessary for its interaction with Foxp3, and either the leucine zipper (LZ) or Forkhead (FKH) domain of Foxp3 is necessary for its interaction with Ahr (fig. S3, F to I). Together, these data demonstrate that Ahr cooperates with Foxp3 potentially via protein-protein interactions at the $Gpr15$ locus to positively regulate $Gpr15$ transcription in Tregs.

RORγt negatively regulates GPR15 expression

RORγt$^+$ Tregs that co-express Ahr are abundantly present in the gut, especially in the large intestine (14), which prompted us to investigate the regulatory effect of RORγt on GPR15. Examination of GPR15 expression in RORγt$^+$ $vs.$ RORγt$^-$ Tregs in the gut revealed that GPR15 expression in RORγt$^-$ Tregs was modestly but significantly higher than those in RORγt$^+$ Tregs (Fig. 4, A and B). In addition, compared to RORγt$^+$ iTregs, RORγt$^-$ iTregs also expressed higher levels of GPR15 (Fig. 4, C and D). Of note, the negative correlation of RORγt and GPR15 expression was apparent in both Ahr–sufficient and –deficient Tregs (Fig. 4, A to D). Furthermore, iTregs and Th17 cells differentiated from RORγt-deficient

CD4^{+} T cells had higher GPR15 expression, compared to those from RORγt-sufficent CD4^{+} T cells (Fig. 4, E to I). Together, these data suggest that RORγt acts a suppressor to inhibit GPR15 expression.

We previously observed a cooperative action of RORγt and Ahr in promoting the expression of IL-22, a cytokine produced by ILC3s and CD4^{+} T cells (23). Thus, we aimed to determine the regulatory effects of RORγt and Ahr on GPR15 expression. To this end, we performed co-transduction of wild-type CD4^{+} T cells with retroviral empty vectors (MIG-EV and MIT-EV) or vectors encoding Ahr-IRES-GFP (MIG-Ahr) and RORγt-IRES-Thy1.1 (MIT-RORγt). We gated on different cell populations that had forced expression of MIG-Ahr (Q1), MIT-RORγt (Q3), or both (Q2) and examined GPR15 expression in each population. While Ahr promoted GPR15 expression (Q1), RORγt markedly suppressed GPR15 expression (Q3) (Fig. 5, A and B). This inhibitory effect of RORγt on GPR15 expression was also evident in the presence of Ahr (Q2), suggesting that RORγt may antagonize Ahr activity at the *Gpr15* locus.

RORγt inhibits Ahr binding activity at the *Gpr15* locus

Examination of previously published ChIP-seq of RORγt in Th17 cells (24) revealed recruitment of RORγt to the open chromatin regions of the *Gpr15* locus (+15 kb and +17 kb, Fig. 2C), where Ahr and Foxp3 co-bound. Moreover, computational analysis (ECR Browser, dCODE) revealed the canonical binding motifs of Ahr and RORγt but not Foxp3 at the *Gpr15* +15 and +17 kb loci (fig. S4A). To determine the crosstalk between Ahr and RORγt in regulation of *Gpr15* in Tregs, we conducted the ChIP assay of Ahr or RORγt in iTregs differentiated from naïve CD4^{+} T cells of RORγt-het (*Rorc*$^{gfp/+}$) and RORγt KO mice (*Rorc*$^{gfp/gfp}$), or those of *Ahr*$^{+/+}$ and *Ahr*$^{-/-}$ mice, respectively. Ahr recruitment to the *Gpr15* locus was modestly but significantly enhanced in the absence of RORγt in iTregs or Th17 cells differentiated from *Rorc*$^{gfp/gfp}$ mice in which RORγt is deficient (Fig. 5C and fig. S4B); while RORγt binding at the *Gpr15* locus was markedly increased without Ahr (Fig. 5D), suggesting a competition between Ahr and RORγt binding to the *Gpr15* locus. To further determine the regulation of Ahr DNA binding at the *Gpr15* locus, we transduced control (MIG-EV), wild-type RORγt or ΔDBD (a mutant RORγt that lacks DNA-binding domain (DBD)) into RORγt-deficient CD4^{+} T cells that were differentiated in iTreg-polarizing condition and then performed an Ahr ChIP assay. Our data showed that transduction of wild-type RORγt but not ΔDBD significantly reduced Ahr binding at the *Gpr15* locus (Fig. S4C). Furthermore, forced expression of wild-type but not ΔDBD in RORγt-deficient iTregs suppressed GPR15 expression (Fig. 5, E and F). Together, these data demonstrate that RORγt negatively regulates GPR15 expression at least in part by competing with Ahr for binding to the opening chromatin regions of the *Gpr15* locus. Of note, co-IP experiment showed that expression of RORγt did not interfere with the interaction of Ahr and Foxp3, but instead co-precipitated with Ahr and Foxp3 (fig. S4D), suggesting that the three proteins might exist in one protein complex, consistent with the previously reported interactions of RORγt with Ahr or Foxp3 (20, 23).

Ahr promotes homing of Tregs to the large intestine by regulating GPR15

To determine the functional relevance of Ahr-mediated GPR15 expression, we performed a short-term homing assay (fig. S5A). Specifically, $Ahr^{+/+}$ and $Ahr^{-/-}$ iTregs were mixed at a 1:1 ratio and transferred into $Rag1^{-/-}$ mice. All tissues examined exhibited approximate similar frequencies of each genotype of the donor-derived cells, except for the large intestine and small intestine, where there was approximately 3-fold fewer Ahr-deficient iTregs relative to wild-type controls (Fig. 6A and fig. S5B). These data are consistent with the role of Ahr in regulating the expression of multiple gut homing and retention molecules (14). Furthermore, we transduced a control (MIG-EV) or a GPR15-encoding retrovirus (MIT-GPR15) into $Ahr^{-/-}$ iTregs (fig. S5C) and transferred them at 1:1 ratio into $Rag1^{-/-}$ mice. Forced expression of GPR15 significantly enhanced Ahr-deficient Tregs homing to the large intestine but not to other organs including the small intestine, consistent with a critical role for GPR15 in Treg large intestinal homing (Fig. 6B and fig. S5D). Furthermore, a comparable homing capacity to the large intestine but not the small intestine between wild-type iTregs and GPR15-restored Ahr-deficient iTregs was observed (Fig. 6C, and fig. S5, E and F), suggesting that impaired expression of GPR15 in Ahr-deficient iTregs is the major mechanism underlying their homing defect to the large intestine.

Previously, we have shown that Ahr-deficient Tregs have impaired suppressive function in CD45RB^{hi} T cell transfer model of colitis (14). We aimed to determine whether forced expression of GPR15 in Ahr-deficient iTregs could rescue their impaired function by guiding them to the large intestine. Since Treg homing to the gut is dispensable for suppressing CD45RB^{hi} T cell transfer-induced colitis (4, 25), we utilized the α-CD40 mediated colitis model (fig. S5G). Consistent with the literature, transferring Tregs could not rescue the systemic wasting disease as revealed by weight loss (ref. (26) and fig. S5H); however, forced expression of GPR15 in Ahr-deficient iTreg promoted their homing to the large intestine during inflammation (Fig. 6D). In addition, adoptive transfer of Ahr-deficient iTregs with forced expression of GPR15 significantly suppressed gut inflammation as revealed by alleviated gut histological changes (Fig. 6, E and F) and reduced proinflammatory cytokine expression (i.e., *Tnf* and *Il1b*) (Fig. 6, G and H). Together, these data demonstrate that Ahr controls large intestine homing of Tregs and their suppression of gut inflammation by positively regulating GPR15 expression.

Ahr signaling promotes GPR15 expression by human Tregs

Given the complex role of GPR15 in human (3, 4), we examined the expression of GPR15 in human colonic Tregs (CD3^{+}CD4^{+}CD45RA^{−}CD45RO^{+}CD127^{−}CD25^{+}Foxp3^{+}) from normal tissues of ulcerative colitis patients. In contrast to a previous report showing minimal expression of GPR15 by human Tregs, we observed its expression in all patient samples. The colonic Tregs had significantly higher expression of GPR15 compared to those in PBMC (Fig. 7, A and B, and fig. S6, A and B). In contrast, the GPR15 expression in Tregs from human small intestine was much lower than that in colonic Tregs (fig. S6C). An increase in *Ahr* mRNA expression in human Tregs was associated with increased *Gpr15* expression as well as increased expression of other Ahr target genes (*Cyp1a1* and *Ahrr*) (Fig. 7, C and D, and fig. S6, D and E), consistent with the role of Ahr in promoting GPR15 expression. Moreover, analysis of GPR15 and Foxp3 expression by protein staining showed

that Foxp3 expression was positively associated with GPR15 expression in human CD127⁻
CD25⁺ T cells (Fig. 7, E and F).

We performed *in vitro* differentiation of iTregs from sorted naïve CD4⁺ T cells
(CD3⁺CD4⁺CD25⁻CD45RA⁺) of human PBMC. The addition of the Ahr ligand FICZ
significantly enhanced the expression of GPR15 and other Ahr target genes but not Ahr,
whereas treatment with CH223191, a specific Ahr antagonist (27), abolished GPR15
expression in human iTregs (Fig. 7, G to K, and fig. S6F). Together, our results
demonstrated a conserved role of Ahr in regulating GPR15 expression in human Tregs.

Discussion

Our previous RNA-seq data showed that Treg-specific ablation of Ahr decreases *Gpr15*
transcription (14), indicating the regulatory effect of Ahr on GPR15 in Tregs. In this study,
we explored the underlying molecular mechanisms and demonstrated that Ahr plays a
pivotal role, which is conserved in mice and human, to positively regulate GPR15 expression
in CD4⁺ T cells, especially in the large intestine under the steady state and during
inflammation. Mechanistically, Ahr binds directly to the open chromatin regions marked by
ATAC-seq peaks at the *Gpr15* locus (+15 kb and +17kb), to control *Gpr15* transcription in
Tregs. These regions also harbor histone epigenetic mark H3K27Ac and H3K4me1 and
likely represent active enhancer(s) of *Gpr15* (fig. S7A and ref. (28)). Genetic ablation of Ahr
did not have a significant impact on chromatin conformational changes at these enhancer
regions but markedly reduced *Gpr15* transcription. These data favor a model that Ahr
directly regulates *Gpr15* transcription by targeting an event downstream of chromatin
remodeling that is likely established by other factors.

Foxp3 is an important transcriptional regulator in Tregs that modulates target genes'
transcription via cooperation with other protein partners (29, 30). Consistent with this
notion, despite lack of Foxp3 DNA-binding consensus sequences at the opening chromatin
regions of *Gpr15* locus (+15 kb and +17 kb), the Ahr-independent recruitment of Foxp3 to
the locus was detected by ChIP assay. Our data showed that Foxp3 interacted with Ahr, and
cooperated with Ahr to promote GPR15 expression. However, Foxp3 DNA-binding ability
was dispensable for its role on GPR15 expression. In agreement, the canonical Foxp3
binding motif was not observed at the *Gpr15* +15 and +17 kb loci where Ahr and RORγt
bound. Thus, these data are consistent with the literature suggesting that Foxp3 is capable to
promote transcription through mechanisms that do not require the presence of the DNA-
binding domain, or alternatively its canonical target motif in the genes of interest (29, 31).
Indeed, despite its dominant negative effect (32) on wild-type Foxp3-driven GITR
expression (8, 33), a Foxp3 mutant (FKH) that does not bind DNA but retains its
interaction with Ahr promoted GPR15 expression similar to wild-type Foxp3. In addition,
Foxp3 enhanced Ahr binding to the enhancer regions of *Gpr15*. These data suggest that a
cooperative regulatory mode between Foxp3 and Ahr is important for GPR15 expression.

Foxp3 binding was observed in the open chromatin regions at the *GPR15* locus in human
Tregs (4, 34). Intriguingly, it was previously reported that no GPR15 expression could be
detected in human colonic Tregs or iTregs, and the strong binding of Foxp3 at the human

Gpr15 locus was proposed to be responsible for the lack of GPR15 expression, based on an assumption that Foxp3 predominantly functions as a transcriptional repressor (4). In contrast, we observed positive correlation between expression of GPR15 and Foxp3 in human colonic Tregs, mirroring GPR15 expression pattern in mouse gut Tregs, consistent with the role of Foxp3 as both transcriptional repressor and activator (30, 35). Precise mechanism(s) remain to be determined and different Ahr expression and/or activity may account for these discrepancies. Indeed, we observed that human iTregs differentiated in the presence of Ahr ligand expressed more GPR15 and inhibition of the Ahr pathway abolished GPR15.

GPR15 is important for lymphocyte homing to the large intestine where RORγt[+] Tregs are most abundantly present (14, 36–38). Unexpectedly, our data showed the inhibitory effect of RORγt on GPR15 expression in both Tregs and Th17 cells. Notably, RORγt[+] Tregs have higher Ahr expression (14) and are most found in the gut (36–38). Thus, the inhibitory effect of RORγt on Ahr-directed GPR15 expression may suggest an intricate balance of these two transcription factors for optimal expression of a gut homing receptor (GPR15) and tissue homeostasis, thus warranting future investigation. We showed here that RORγt inhibited Ahr recruitment to the *Gpr15* locus, in contrast to our previous observation that RORγt interacts with Ahr, thus promoting Ahr recruitment to the *Il22* locus to direct its transcription (23). Therefore, the consequence of Ahr-RORγt crosstalk in transcriptional regulation is target gene-specific and/or cell type-specific. Modulation of Ahr-RORγt crosstalk may have distinct effects on immune homeostasis and inflammation. Collectively, our data demonstrate an important regulatory axis that involves interactions among Ahr, Foxp3 and RORγt in regulation of GPR15 expression and thus CD4^{+} T cell gut homing (fig. S7B).

Notably, there are less intestinal CD8^{+} T cells in GPR15-deficient mice (3), suggesting that GPR15 may be involved in CD8^{+} T cell gut homing. However, despite the expression of Ahr in CD8^{+} T cells, genetic deletion or activation of Ahr did not affect GPR15 expression in CD8^{+} T cells, suggesting an Ahr-independent mechanism that supports GPR15-expressing CD8^{+} T cells that remains to be determined. The evolutionarily conserved regulatory effect of Ahr on GPR15 between mouse and human highlights a critical role of Ahr to regulate Treg cell gut homing across species and suggests a potential target for the clinical intervention in gut inflammatory diseases. Targeting Ahr-dependent pathway, for example promoting Ahr expression and/or activity to enhance GPR15 expression could be exploited to treat intestinal inflammatory diseases. Intriguingly, it has been observed that the fecal samples from healthy subjects induce greater Ahr activity than those from patients with inflammatory bowel disease (IBD) (39). It remains to be determined whether IBD patients with reduced Ahr-activating microbiota have perturbed Ahr expression in Tregs in the gut. Furthermore, the nature/affinity of ligands of Ahr in mice and human might be different (40), and the role of Ahr in regulating GPR15 expression in health and disease, especially through ligand modulation thus needs to be further determined in human.

Materials and Methods

Study design

The goal of this study was to understand the molecular mechanisms of action of Ahr in regulation of GPR15 expression and gut homing of $CD4^+$ T lymphocytes. Genetic and pharmacologic manipulation of Ahr expression and activity were used to understand how Ahr regulated GPR15 protein and mRNA expression by FACS, and/or real-time RT-PCR. We determined the role of Ahr in the regulation of *Gpr15* transcription by ChIP-seq and ChIP-PCR approaches and *in vitro* transcription reporter assays. We delineate crosstalk among Ahr, Foxp3 and RORγt using co-IP assays and retroviral transduction experiments. The functional relevance of Ahr regulation of GPR15 expression in Tregs was further determined using the anti-CD40 induced colitis model, and the histology of colon sections was blindly analyzed and scored by a trained gastrointestinal pathologist. Four to eight mice (6 to 8 weeks) were used in each group for murine studies and these experiments were repeated at least twice. To reduce bias, mice used in this study were randomized into experimental groups. Experiments were repeated with a different pool of breeding pairs. To improve precision and reduce variability, experiments included multiple biological and technical replicates, and results were analyzed using appropriate statistical methods as described in the methods and figure legends. The specific number of mice or samples used, or the experimental repeats performed, are detailed in the figure legends. The regulatory mechanism was further verified in human samples, including buffy coat-derived PBMCs from healthy donors and tissue biopsies from recruited healthy patients.

Mice

All mice in this study were maintained in specific-pathogen-free (SPF) facilities at the University of Florida. Mice (both sexes) were littermates and were 6–8 weeks old unless otherwise indicated in the text. $Ahr^{-/-}$ (41), Ahr^{CAIR} and $Foxp3^{Yfp-Cre}$ (14), $Rorc^{gfp/gfp}$ (42) mice were previously described. $Ahr^{f/f}$ mice were purchased from Jackson Laboratory. All studies with mice were approved by the Animal Care and Use Committee of the University of Florida.

Human sample collection

Buffy coat-derived PBMCs from healthy donors were purchased from Life South Blood in accordance with the Institutional Review Boards at the University of Florida (UF IRB# 201801563). Healthy patients and patients (both genders) diagnosed with an inflammatory bowel disease (Crohn's disease and ulcerative colitis) were recruited for this study. Patients were at least 18 years old. Patients were recruited during clinical visits to the Inflammatory Bowel and Celiac Disease Program or before an already scheduled colonoscopy. Tissue biopsies were taken from the small intestine (terminal ileum) and/or colon. The mucosa was assessed based on frequently used scoring systems (Mayo score for UC and SES-CD score for CD). Biopsies labeled as "healthy" display normal vascularity and lack the presence of edema, erythema, friability, erosions or ulcerations macroscopically. Intestinal tissue biopsies were collected in RPMI following informed consent in accordance with the Institutional Review Boards at the University of Florida (UF IRB# 201601218) then

immediately processed to isolate lamina propria lymphocytes (LPLs) as described previously (43).

Isolation of intestinal LPLs and flow cytometry

Isolation of intestinal LPLs and flow cytometry were done as described previously (23). Antibodies were purchased from eBioscience, BD Pharmingen, BioLegend, or TONBO. CD16/32 antibody was used to block nonspecific binding to Fc receptors before all surface staining. Sample acquisition was performed on FACSCantoII (BD Biosciences) and analyzed with FlowJo (version 10.2, Tree Star). Method details and gating strategy were described in figure legends and supplemental methods.

Real-Time RT-PCR

RNA of sorted cells or *in vitro* cultured cells was isolated with Trizol (Invitrogen). cDNA was synthesized using the GoScript reverse transcription kit (Promega). Real-time RT-PCR was performed using SYBR Green (Bio-Rad) and various primer sets (Table. S1). Reactions were run using CFX Connect (Bio-Rad). The mRNA levels of target genes were calculated by the comparative C_T ($2^{-\Delta Ct}$) method (44) and normalized to β-actin.

In vitro iTreg and Th17 differentiation

Naïve CD4$^+$ T cells were purified from splenocytes using mouse CD4$^+$ T cell isolation kit (Stemcell Technologies), and further sorted by FACS Aria II (BD Biosciences). 24-well plates were coated with 40 μg/ml anti-hamster antibody (MP Biomedical) at 37°C for 4 hours. For iTreg differentiation, naïve CD4$^+$ T cells were cultured in T cell media IMDM (Sigma-Aldrich) supplemented with soluble 0.25 μg/ml anti-mouse CD3 (145–2C11), 1 μg/ml anti-mouse CD28 (37.51), 2 μg/ml anti-mouse IL-4 (11B11), 2 μg/ml anti-mouse IFN-γ (XMG1.2) and 5 ng/ml TGF-β, with (Th17) or without (iTreg) 20 ng/ml IL-6, for 3.5 days. For human cells, naïve T cells were enriched using the human CD4$^+$ T cell isolation kit (Stemcell) from human PBMC cells and further sorted (CD3$^+$CD4$^+$CD45RA$^+$CD25$^-$). For iTreg differentiation, the sorted naïve human CD4$^+$ T cells were seeded into 48-well plates precoated with 1 μg/mL anti-CD3 antibody (clone HIT3a), and cultured in RPMI media (Sigma-Aldrich) supplemented with IL-2 (10 ng/ml), soluble anti-CD28 (1 μg/ml; clone CD28.2) and 5 ng/ml TGF-β for 6 days. In some experiments, FICZ was added at a concentration of 200 nM as indicated in the text.

Retroviral transduction

The cDNAs of target genes were cloned into MSCV-IRES-Thy1.1 (MIT) or MSCV-IRES-GFP (MIG) retroviral vectors. HEK293T cells were transfected with retroviral plasmids and the packaging plasmid 10A1 using polyethylenimine (PEI). Viral supernatant was collected after transfection. Sorted naïve CD4$^+$ T cells were stimulated on day 0 under neutral (Th0) conditions (plate-coated anti-CD3ε (2C11, 2 μg/ml) and anti-CD28 (37.51, 0.5 μg/ml) antibodies, and 10% FBS in IMDM. After 24 h of culture, retrovirus-containing supernatants supplemented with polybrene (8 μg/ml, Sigma) were added to the cells followed by centrifugation at 2,500 rpm for 2 h at 30°C on day 1 and 2. The cells were further cultured

under Th0 conditions or iTreg differentiation condition before harvest as indicated in the text.

Chromatin immunoprecipitation (ChIP) assay and ChIP-seq

Th17 and iTreg were differentiated from sorted naïve mouse CD4$^+$ T cells as described above. For ChIP of Ahr, cells were treated with FICZ (200 nM) for 4 hours before harvest. Cells were cross-linked with 1% formaldehyde for 15 min. Chromatin was sheared by sonication with Bioruptor Pico (30" on and 30" off for 25 cycles) and immunoprecipitated with anti-Ahr (Enzo Life Science, BML-SA210–0100), anti-RORγt (eBioscience, 14–6988-82) or anti-Foxp3 (Abcam, ab150743) using iDeal ChIP-Seq Kit for transcription factors or True MicroChIP kit (Diagenode). Eluted DNA was used for real-time PCR analyses using specific primers (Table. S1). Samples were sequenced as 50 bp single-end reads.

ChIP-seq, ATAC-seq, and RNA-seq data analysis

For Ahr ChIP-seq 39–52 million raw reads were sequenced. FASTQC was used to ensure maximum per base sequence quality of sequenced data. For all ChIP-seq data sets including the publically available FoxP3 and RORγt ChIP-seq as well as our previously published ATAC-seq, reads were mapped to the mouse genome (mm9) with bowtie2 (v2.3.3) (45) and further filtered using samtools (v1.7) (46). The uniquely aligned reads were used to generate bedgraph files (scaled to 10 million reads) using bedtools (v2.25.0) (47). Genome visualization tracks (bedgraph files) were uploaded to UCSC Genome Browser for visual comparison of expression levels (48, 49). To identify peaks and calculate tag counts from ChIP-seq reads, HOMER (v4.9.1) (50) was used with default parameters. Briefly, to cater to transcription factor binding -style factor was used with peak calling parameters: fold-enrichment over KO = 4, poisson p-value over local region = 0.0001, and FDR 0.05. The Normalized Tag Counts defined as "the number of tags found at the peak, normalized to 10 million total mapped tags" was acquired from the HOMER peak file then sorted and visualized using Excel. The data analyses for RNA-seq and ATAC-seq were described in our previous publication (14), and details can be found in supplemental materials.

Plasmids

cDNA of mouse Ahr (1–805aa) was cloned into MIG with HA or FLAG tag at the N terminus. cDNA of mouse Foxp3 (1–429aa) was cloned into MIG with FLAG tag. cDNA of mouse RORγt (1–495aa) was cloned into MIG or MIT, and the RORγt DBD (81–495aa) were subcloned into pMIR-DFTC (double Flag-tagged). cDNA of mouse GPR15 (1–360aa) was cloned into MIT. The Ahr Y9A (1–805aa, Y9A), Ahr bHLH (1–120aa were deleted), Ahr AD (425–805aa), Ahr AD (1–424aa), Ahr PAS (121–424aa were deleted), Ahr PASA (121–276aa were deleted) and Ahr PASB (276–424aa were deleted) were subcloned into MIG with HA tag. The Foxp3 mutants including Foxp3 (70–429aa), Foxp3 (195–429aa), Foxp3 (235–429aa), Foxp3 FKH (1–328aa), Foxp3 (1–265aa), Foxp3 (1–225aa), Foxp3 LZ (226–265aa were deleted), Foxp3 Ex2 (70–105aa were deleted) and Foxp3 Ex2 FKH (70–105aa and 329–429aa were deleted) were subcloned into MIG with FLAG tag.

Transient transfection, immunoprecipitation, and Western blot

HEK 293T cells were transfected with the indicated constructs using polyethylenimine (PEI). Forty-eight hours after transfection, whole-cell extracts were made in lysis buffer (50 mM Tris-HCl (pH 8.0), 120 mM NaCl, 4 mM EDTA, 1% NP40, 1 mM DTT) with protease inhibitor cocktails (Roche). After the insoluble material was removed by centrifugation, the lysate was immunoprecipitated with corresponding antibodies at 4°C for 3 hours and subjected to SDS-PAGE and immunoblotting with the indicated antibodies.

Ahr ligand deficient diet treatment

Littermate pups were weaned at 3 weeks old into two separate cages and fed with the Ahr ligand-deficient diet (AIN-76A, Envigo) or AIN-76A with addition at a concentration of 2g/kg Ahr ligand I3C (76A+ I3C) for three weeks before the analysis.

Competitive homing assay

Naïve CD4$^+$ T cells were sorted from the spleens of $Ahr^{+/+}$ (CD45.1/45.1 or CD45.2/45.2) or $Ahr^{-/-}$ (CD45.2/45.2) mice and *in vitro* differentiated to iTreg as indicated above. Or, the sorted naïve CD4$^+$ T cells were transduced with a control (MIG-EV/MIT-EV) or a GPR15-encoding retrovirus at day 1 and day 2 after stimulation with anti-mouse CD3 (145–2C11) and 1 μg/ml anti-mouse CD28, and then *in vitro* differentiated into iTreg. Tregs were mixed at a 1:1 ratio and $1–2 \times 10^7$ mixed cells were adoptively transferred into $Rag1^{-/-}$ mice, and migration of donor cells into each organ was determined 10 hours after transfer.

α-CD40 antibody-induced inflammation/colitis and rescue by Treg transfer

Naïve CD4$^+$ T cells were sorted from the spleen of $Ahr^{f/+} Foxp3^{Yfp-Cre}$ or $Ahr^{f/-} Foxp3^{Yfp-Cre}$ littermate mice and transduced with control (MIT-EV) or GPR15-encoding retrovirus (GPR15), which was then *in vitro* differentiated to iTreg. MIT$^+$Tregs were further sorted and transferred intravenously to $Rag1^{-/-}$ recipients. 3 weeks later, mice were injected with α-CD40 (FGK 45) antibody (50 μg i.p.) and colonic tissues were examined at day 2 after antibody injection. Tissues were processed for H&E staining as described above.

Histological Analysis

Tissue samples handling and histology scoring was performed as previously described (51). Briefly, tissues from proximal colon were dissected and fixed with formalin. Tissues were then embedded in paraffin, sectioned and stained with hematoxylin and eosin (H&E). Sections were then blindly analyzed by a trained gastrointestinal pathologist and the histology scores were given based on a previously described standard (31). The seven parameters used include (1) lamina propria inflammation (0–3), (2) goblet cell loss (0–2), (3) abnormal crypts (0–3), (4) crypt abscesses (0–1), (5) mucosal erosion or ulceration (0–1), (6) submucosal spread to transmural inflammation (0–4), and (7) neutrophil counts (0–4). The sum of the scores in each parameter was used to evaluate the inflammatory severity in the sections.

Statistical methods

Unless otherwise noted, statistical analysis was performed with unpaired Student's t test (for comparisons of two groups) on individual biological samples, or one-way analysis of variance (ANOVA) analysis (for comparison of three or more groups) with GraphPad Prism. Results were expressed as mean ± SEM. *p 0.05, **p 0.01, ***p 0.001, ****p 0.0001, ns: nonsignificant statistical differences.

Supplementary Material

Refer to Web version on PubMed Central for supplementary material.

Acknowledgements

References and Notes

1. Heiber M, Marchese A, Nguyen T, Heng HH, George SR, O'Dowd BF, A novel human gene encoding a G-protein-coupled receptor (GPR15) is located on chromosome 3. Genomics 32, 462–465 (1996). [PubMed: 8838812]

2. Deng HK, Unutmaz D, KewalRamani VN, Littman DR, Expression cloning of new receptors used by simian and human immunodeficiency viruses. Nature 388, 296–300 (1997). [PubMed: 9230441]

3. Kim SV, Xiang WV, Kwak C, Yang Y, Lin XW, Ota M, Sarpel U, Rifkin DB, Xu R, Littman DR, GPR15-mediated homing controls immune homeostasis in the large intestine mucosa. Science 340, 1456–1459 (2013). [PubMed: 23661644]

4. Nguyen LP, Pan J, Dinh TT, Hadeiba H, O'Hara E 3rd, Ebtikar A, Hertweck A, Gokmen MR, Lord GM, Jenner RG, Butcher EC, Habtezion A, Role and species-specific expression of colon T cell homing receptor GPR15 in colitis. Nat. Immunol. 16, 207–213 (2015). [PubMed: 25531831]

5. Suply T, Hannedouche S, Carte N, Li J, Grosshans B, Schaefer M, Raad L, Beck V, Vidal S, Hiou-Feige A, Beluch N, Barbieri S, Wirsching J, Lageyre N, Hillger F, Debon C, Dawson J, Smith P, Lannoy V, Detheux M, Bitsch F, Falchetto R, Bouwmeester T, Porter J, Baumgarten B, Mansfield K, Carballido JM, Seuwen K, Bassilana F, A natural ligand for the orphan receptor GPR15 modulates lymphocyte recruitment to epithelia. Sci. Signal. 10, (2017).

6. Lahl K, Sweere J, Pan J, Butcher E, Orphan chemoattractant receptor GPR15 mediates dendritic epidermal T-cell recruitment to the skin. Eur. J. Immunol. 44, 2577–2581 (2014). [PubMed: 24838826]

7. Sezin T, Kempen L, Meyne LM, Mousavi S, Zillikens D, Sadik CD, GPR15 is not critically involved in the regulation of murine psoriasiform dermatitis. J. Dermatol. Sci. 94, 196–204 (2019). [PubMed: 30935778]

8. Marson A, Kretschmer K, Frampton GM, Jacobsen ES, Polansky JK, MacIsaac KD, Levine SS, Fraenkel E, von Boehmer H, Young RA, Foxp3 occupancy and regulation of key target genes during T-cell stimulation. Nature 445, 931–935 (2007). [PubMed: 17237765]

9. Zheng Y, Josefowicz SZ, Kas A, Chu TT, Gavin MA, Rudensky AY, Genome-wide analysis of Foxp3 target genes in developing and mature regulatory T cells. Nature 445, 936–940 (2007). [PubMed: 17237761]

10. Stockinger B, Di Meglio P, Gialitakis M, Duarte JH, The aryl hydrocarbon receptor: multitasking in the immune system. Annu. Rev. Immunol. 32, 403–432 (2014). [PubMed: 24655296]

11. Zhou L, AHR Function in Lymphocytes: Emerging Concepts. Trends Immunol. 37, 17–31 (2016). [PubMed: 26700314]

12. Cella M, Colonna M, Aryl hydrocarbon receptor: Linking environment to immunity. Semin. Immunol. 27, 310–314 (2015). [PubMed: 26561251]

13. Rothhammer V, Quintana FJ, The aryl hydrocarbon receptor: an environmental sensor integrating immune responses in health and disease. Nat. Rev. Immunol. 19, 184–197 (2019). [PubMed: 30718831]

14. Ye J, Qiu J, Bostick JW, Ueda A, Schjerven H, Li S, Jobin C, Chen ZE, Zhou L, The Aryl Hydrocarbon Receptor Preferentially Marks and Promotes Gut Regulatory T Cells. Cell Rep. 21, 2277–2290 (2017). [PubMed: 29166616]

15. Li Y, Innocentin S, Withers DR, Roberts NA, Gallagher AR, Grigorieva EF, Wilhelm C, Veldhoen M, Exogenous stimuli maintain intraepithelial lymphocytes via aryl hydrocarbon receptor activation. Cell 147, 629–640 (2011). [PubMed: 21999944]

16. Esser C, Rannug A, Stockinger B, The aryl hydrocarbon receptor in immunity. Trends Immunol. 30, 447–454 (2009). [PubMed: 19699679]

17. Li S, Bostick JW, Zhou L, Regulation of Innate Lymphoid Cells by Aryl Hydrocarbon Receptor. Front. Immunol. 8, 1909 (2017). [PubMed: 29354125]

18. Hankinson O, Role of coactivators in transcriptional activation by the aryl hydrocarbon receptor. Arch. Biochem. Biophys. 433, 379–386 (2005). [PubMed: 15581594]

19. Swanson HI, Yang J, Mapping the protein/DNA contact sites of the Ah receptor and Ah receptor nuclear translocator. J. Biol. Chem. 271, 31657–31665 (1996). [PubMed: 8940186]

20. Zhou L, Lopes JE, Chong MM, Ivanov II, Min R, Victora GD, Shen Y, Du J, Rubtsov YP, Rudensky AY, Ziegler SF, Littman DR, TGF-beta-induced Foxp3 inhibits T(H)17 cell differentiation by antagonizing RORgammat function. Nature 453, 236–240 (2008). [PubMed: 18368049]

21. Chen R, Belanger S, Frederick MA, Li B, Johnston RJ, Xiao N, Liu YC, Sharma S, Peters B, Rao A, Crotty S, Pipkin ME, In vivo RNA interference screens identify regulators of antiviral CD4(+) and CD8(+) T cell differentiation. Immunity 41, 325–338 (2014). [PubMed: 25148027]

22. Hayatsu N, Miyao T, Tachibana M, Murakami R, Kimura A, Kato T, Kawakami E, Endo TA, Setoguchi R, Watarai H, Nishikawa T, Yasuda T, Yoshida H, Hori S, Analyses of a Mutant Foxp3 Allele Reveal BATF as a Critical Transcription Factor in the Differentiation and Accumulation of Tissue Regulatory T Cells. Immunity 47, 268–283 e269 (2017). [PubMed: 28778586]

23. Qiu J, Heller JJ, Guo X, Chen ZM, Fish K, Fu YX, Zhou L, The aryl hydrocarbon receptor regulates gut immunity through modulation of innate lymphoid cells. Immunity 36, 92–104 (2012). [PubMed: 22177117]

24. Ciofani M, Madar A, Galan C, Sellars M, Mace K, Pauli F, Agarwal A, Huang W, Parkhurst CN, Muratet M, Newberry KM, Meadows S, Greenfield A, Yang Y, Jain P, Kirigin FK, Birchmeier C, Wagner EF, Murphy KM, Myers RM, Bonneau R, Littman DR, A validated regulatory network for Th17 cell specification. Cell 151, 289–303 (2012). [PubMed: 23021777]

25. Denning TL, Kim G, Kronenberg M, Cutting edge: CD4+CD25+ regulatory T cells impaired for intestinal homing can prevent colitis. J. Immunol. 174, 7487–7491 (2005). [PubMed: 15944246]

26. Bauche D, Joyce-Shaikh B, Jain R, Grein J, Ku KS, Blumenschein WM, Ganal-Vonarburg SC, Wilson DC, McClanahan TK, Malefyt RW, Macpherson AJ, Annamalai L, Yearley JH, Cua DJ, LAG3(+) Regulatory T Cells Restrain Interleukin-23-Producing CX3CR1(+) Gut-Resident Macrophages during Group 3 Innate Lymphoid Cell-Driven Colitis. Immunity 49, 342–352 e345 (2018). [PubMed: 30097293]

27. Kim SH, Henry EC, Kim DK, Kim YH, Shin KJ, Han MS, Lee TG, Kang JK, Gasiewicz TA, Ryu SH, Suh PG, Novel compound 2-methyl-2H-pyrazole-3-carboxylic acid (2-methyl-4-o-tolylazo-phenyl)-amide (CH-223191) prevents 2,3,7,8-TCDD-induced toxicity by antagonizing the aryl hydrocarbon receptor. Mol. Pharmacol. 69, 1871–1878 (2006). [PubMed: 16540597]

28. van der Veeken J, Gonzalez AJ, Cho H, Arvey A, Hemmers S, Leslie CS, Rudensky AY, Memory of Inflammation in Regulatory T Cells. Cell 166, 977–990 (2016). [PubMed: 27499023]

29. Samstein RM, Arvey A, Josefowicz SZ, Peng X, Reynolds A, Sandstrom R, Neph S, Sabo P, Kim JM, Liao W, Li MO, Leslie C, Stamatoyannopoulos JA, Rudensky AY, Foxp3 exploits a pre-

existent enhancer landscape for regulatory T cell lineage specification. Cell 151, 153–166 (2012). [PubMed: 23021222]

30. Rudra D, deRoos P, Chaudhry A, Niec RE, Arvey A, Samstein RM, Leslie C, Shaffer SA, Goodlett DR, Rudensky AY, Transcription factor Foxp3 and its protein partners form a complex regulatory network. Nat. Immunol. 13, 1010–1019 (2012). [PubMed: 22922362]

31. Pavlick KP, Ostanin DV, Furr KL, Laroux FS, Brown CM, Gray L, Kevil CG, Grisham MB, Role of T-cell-associated lymphocyte function-associated antigen-1 in the pathogenesis of experimental colitis. Int. Immunol. 18, 389–398 (2006). [PubMed: 16415103]

32. Park JH, Ko JS, Shin Y, Cho JY, Oh HA, Bothwell AL, Lee SK, Intranuclear interactomic inhibition of FoxP3 suppresses functions of Treg cells. Biochem. Biophys. Res. Commun. 451, 1–7 (2014). [PubMed: 25044110]

33. Kwon HK, Chen HM, Mathis D, Benoist C, FoxP3 scanning mutagenesis reveals functional variegation and mild mutations with atypical autoimmune phenotypes. Proc. Natl. Acad. Sci. U. S. A. 115, E253–E262 (2018). [PubMed: 29269391]

34. Birzele F, Fauti T, Stahl H, Lenter MC, Simon E, Knebel D, Weith A, Hildebrandt T, Mennerich D, Next-generation insights into regulatory T cells: expression profiling and FoxP3 occupancy in Human. Nucleic Acids Res. 39, 7946–7960 (2011). [PubMed: 21729870]

35. Lu L, Barbi J, Pan F, The regulation of immune tolerance by FOXP3. Nat. Rev. Immunol. 17, 703–717 (2017). [PubMed: 28757603]

36. Ohnmacht C, Park JH, Cording S, Wing JB, Atarashi K, Obata Y, Gaboriau-Routhiau V, Marques R, Dulauroy S, Fedoseeva M, Busslinger M, Cerf-Bensussan N, Boneca IG, Voehringer D, Hase K, Honda K, Sakaguchi S, Eberl G, MUCOSAL IMMUNOLOGY. The microbiota regulates type 2 immunity through RORgammat(+) T cells. Science 349, 989–993 (2015). [PubMed: 26160380]

37. Sefik E, Geva-Zatorsky N, Oh S, Konnikova L, Zemmour D, McGuire AM, Burzyn D, Ortiz-Lopez A, Lobera M, Yang J, Ghosh S, Earl A, Snapper SB, Jupp R, Kasper D, Mathis D, Benoist C, MUCOSAL IMMUNOLOGY. Individual intestinal symbionts induce a distinct population of RORgamma(+) regulatory T cells. Science 349, 993–997 (2015). [PubMed: 26272906]

38. Kim KS, Hong SW, Han D, Yi J, Jung J, Yang BG, Lee JY, Lee M, Surh CD, Dietary antigens limit mucosal immunity by inducing regulatory T cells in the small intestine. Science 351, 858–863 (2016). [PubMed: 26822607]

39. Lamas B, Richard ML, Leducq V, Pham HP, Michel ML, Da Costa G, Bridonneau C, Jegou S, Hoffmann TW, Natividad JM, Brot L, Taleb S, Couturier-Maillard A, Nion-Larmurier I, Merabtene F, Seksik P, Bourrier A, Cosnes J, Ryffel B, Beaugerie L, Launay JM, Langella P, Xavier RJ, Sokol H, CARD9 impacts colitis by altering gut microbiota metabolism of tryptophan into aryl hydrocarbon receptor ligands. Nat. Med. 22, 598–605 (2016). [PubMed: 27158904]

40. Ramadoss P, Perdew GH, Use of 2-azido-3-[125I]iodo-7,8-dibromodibenzo-p-dioxin as a probe to determine the relative ligand affinity of human versus mouse aryl hydrocarbon receptor in cultured cells. Mol. Pharmacol. 66, 129–136 (2004). [PubMed: 15213304]

41. Fernandez-Salguero P, Pineau T, Hilbert DM, McPhail T, Lee SS, Kimura S, Nebert DW, Rudikoff S, Ward JM, Gonzalez FJ, Immune system impairment and hepatic fibrosis in mice lacking the dioxin-binding Ah receptor. Science 268, 722–726 (1995). [PubMed: 7732381]

42. Eberl G, Marmon S, Sunshine MJ, Rennert PD, Choi Y, Littman DR, An essential function for the nuclear receptor RORgamma(t) in the generation of fetal lymphoid tissue inducer cells. Nat. Immunol. 5, 64–73 (2004). [PubMed: 14691482]

43. Bowcutt R, Malter LB, Chen LA, Wolff MJ, Robertson I, Rifkin DB, Poles M, Cho I, Loke P, Isolation and cytokine analysis of lamina propria lymphocytes from mucosal biopsies of the human colon. J. Immunol. Methods 421, 27–35 (2015). [PubMed: 25769417]

44. Livak KJ, Schmittgen TD, Analysis of relative gene expression data using real-time quantitative PCR and the 2(-Delta Delta C(T)) Method. Methods 25, 402–408 (2001). [PubMed: 11846609]

45. Langmead B, Salzberg SL, Fast gapped-read alignment with Bowtie 2. Nat. Methods 9, 357–359 (2012). [PubMed: 22388286]

46. Li H, Handsaker B, Wysoker A, Fennell T, Ruan J, Homer N, Marth G, Abecasis G, Durbin R, The Sequence Alignment/Map format and SAMtools. Bioinformatics 25, 2078–2079 (2009). [PubMed: 19505943]

47. Quinlan AR, Hall IM, BEDTools: a flexible suite of utilities for comparing genomic features. Bioinformatics 26, 841–842 (2010). [PubMed: 20110278]

48. Meyer LR, Zweig AS, Hinrichs AS, Karolchik D, Kuhn RM, Wong M, Sloan CA, Rosenbloom KR, Roe G, Rhead B, Raney BJ, Pohl A, Malladi VS, Li CH, Lee BT, Learned K, Kirkup V, Hsu F, Heitner S, Harte RA, Haeussler M, Guruvadoo L, Goldman M, Giardine BM, Fujita PA, Dreszer TR, Diekhans M, Cline MS, Clawson H, Barber GP, Haussler D, Kent WJ, The UCSC Genome Browser database: extensions and updates 2013. Nucleic Acids Res. 41, D64–69 (2013). [PubMed: 23155063]

49. Patel RK, Jain M, NGS QC Toolkit: a toolkit for quality control of next generation sequencing data. PLoS One 7, e30619 (2012). [PubMed: 22312429]

50. Heinz S, Benner C, Spann N, Bertolino E, Lin YC, Laslo P, Cheng JX, Murre C, Singh H, Glass CK, Simple combinations of lineage-determining transcription factors prime cis-regulatory elements required for macrophage and B cell identities. Mol. Cell 38, 576–589 (2010). [PubMed: 20513432]

51. Qiu J, Guo X, Chen ZM, He L, Sonnenberg GF, Artis D, Fu YX, Zhou L, Group 3 innate lymphoid cells inhibit T-cell-mediated intestinal inflammation through aryl hydrocarbon receptor signaling and regulation of microflora. Immunity 39, 386–399 (2013). [PubMed: 23954130]
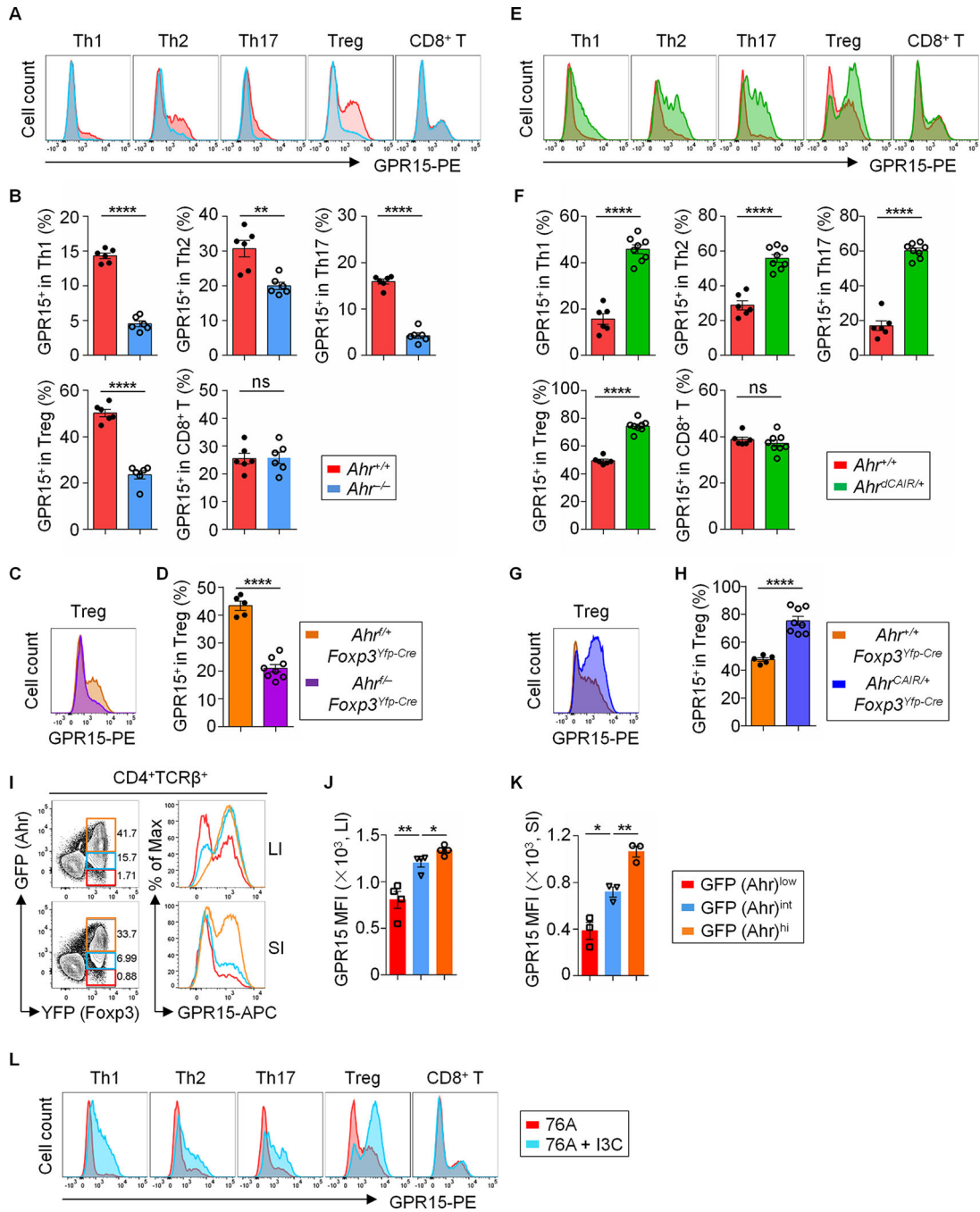
Fig. 1. GPR15 in CD4+ T cells is most prominently expressed by large intestinal Tregs and controlled by Ahr.

(**A**) Flow cytometry analysis of GPR15 expression in Th1 (CD4+TCRβ+Foxp3−GATA3−T-bet+), Th2 (CD4+TCRβ+Foxp3−GATA3+), Th17 (CD4+TCRβ+Foxp3−GATA3−RORγt+), Treg (CD4+TCRβ+Foxp3+) and CD8+ (CD8+TCRβ+) T cells isolated from lamina propria of the large intestine (LI) of $Ahr^{+/+}$ and $Ahr^{−/−}$ littermate mice. Data are representative of four independent experiments. (**B**) Percentages of the GPR15+ proportion among Th1/Th2/Th17/Treg/CD8+ T cells from LI of $Ahr^{+/+}$ and $Ahr^{−/−}$ littermate mice. Data are shown as

mean ± SEM (n =6 mice per group). (**C**) Flow cytometry analysis of GPR15 expression in Tregs from LI of the indicated littermate mice. Data are representative of three independent experiments. (**D**) Percentages of GPR15$^+$ proportion in Tregs from LI of the indicated littermate mice. Data are shown as mean ± SEM (n = 5–8 mice per group). (**E**) Flow cytometry analysis of GPR15 expression in Th1, Th2, Th17, Treg and CD8$^+$ T cells from LI of *Ahr$^{+/+}$* and *Ahr$^{dCAIR/+}$* littermate mice. Data are representative of three independent experiments. (**F**) Percentages of the GPR15$^+$ proportion among Th1/Th2/Th17/Treg/CD8$^+$ T cells from LI of the indicated littermate mice. Data are shown as mean ± SEM (n = 6–8 mice per group). (**G**) Flow cytometry analysis of GPR15 expression in Tregs from LI of the indicated littermate mice. Data are representative of three independent experiments. (**H**) Percentages of GPR15$^+$ proportion in Tregs from LI of the indicated littermate mice. Data are shown as mean ± SEM (n = 5–8 mice per group). (**I**) The expression of GPR15 by each individual Treg population corresponding to different levels of *Ahr* expression (GFP), depicted in color (i.e., orange, blue and red; left column) was analyzed by flow cytometry (right column). Data are representative of two independent experiments. The compiled data for MFI (mean fluorescence intensity) of GPR15 expression in each individual Treg population corresponding to different levels of *Ahr* expression (GFP) from LI (**J**) and SI (**K**) was shown as mean ± SEM (n = 3–4 mice per group). (**L**) Flow cytometry analysis of GPR15 expression by Th1/Th2/Th17/Treg/CD8$^+$ T cells in LI of littermate C57BL/6 wild-type mice fed with Ahr ligand-deficient diet (AIN-76A) or AIN–76A with addition of Ahr ligand I3C (76A+ I3C). Data are representative of two independent experiments. Also see fig. S1 and S2, and Table S2.
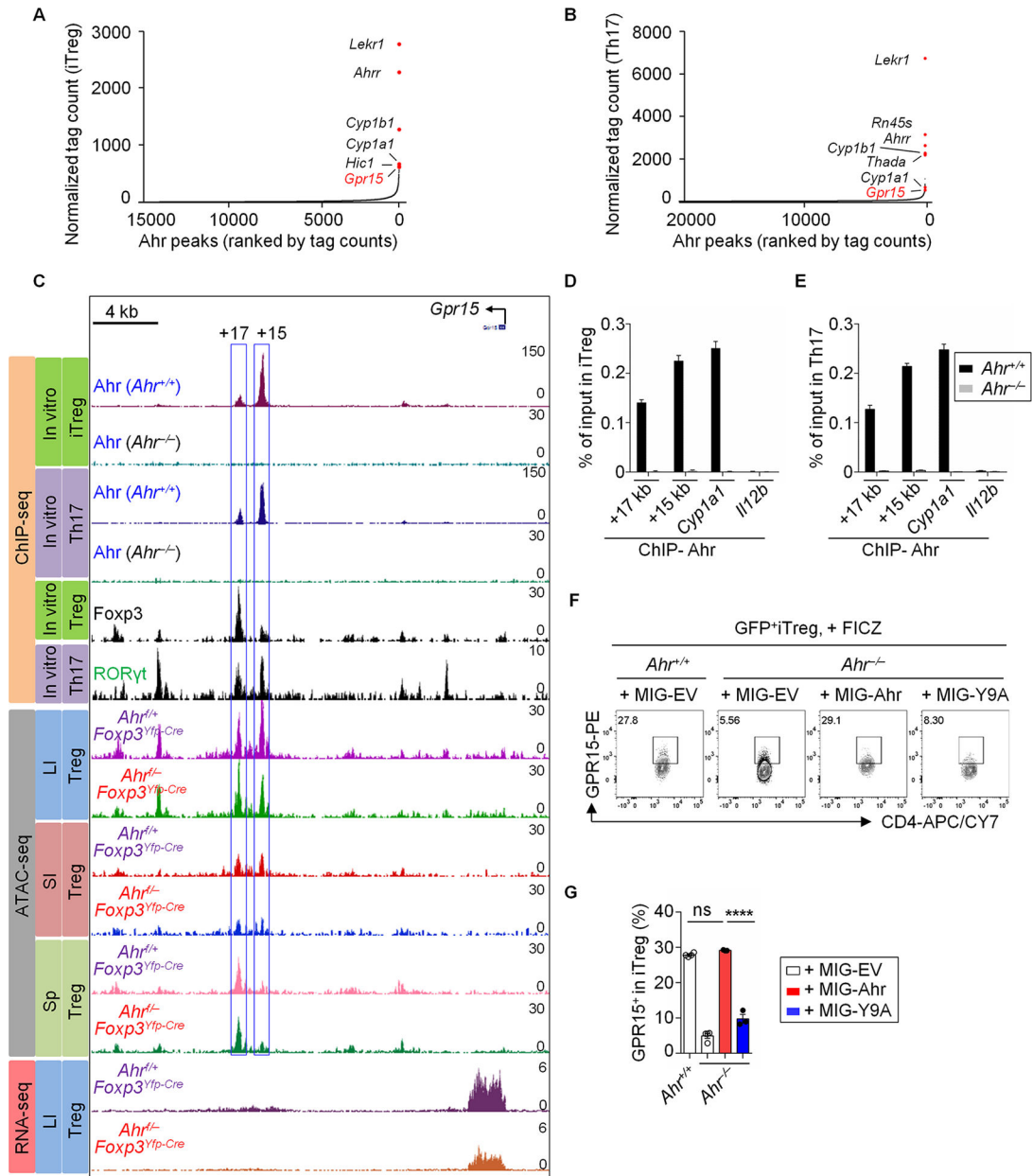
Fig. 2. Ahr regulates GPR15 expression by directly binding to the *Gpr15* locus.
(**A** and **B**) Ranking of Ahr binding intensity at high-confidence regions from ChIP-seq in iTreg (**A**) or Th17 (**B**). (**C**) ChIP-seq: recruitment of Ahr, Foxp3 or RORγt to the *Gpr15* locus in iTregs and/or Th17, as measured by ChIP-seq in this study (for Ahr) or published ChIP-seq data (for Foxp3 and RORγt). ATAC-seq: representative ATAC-seq tracks at the *Gpr15* locus in Tregs sorted from the LI, SI or Sp of *Ahr^f/+ Foxp3^Yfp-Cre* or *Ahr^f/− Foxp3^Yfp-Cre* littermate mice. RNA-seq: representative RNA-seq tracks at the *Gpr15* locus in Tregs sorted from the LI of *Ahr^f/+ Foxp3^Yfp-Cre* or *Ahr^f/−Foxp3^Yfp-Cre* littermate mice. (**D** and **E**) ChIP assay of iTreg (**D**) and Th17 (**E**) from *Ahr^+/+* or *Ahr^−/−* littermate mice. Enrichment of Ahr at the site 17 kb (+17 kb) or 15 kb (+15 kb) downstream of the transcription start site of *Gpr15* was determined by real-time PCR. Data are representative of
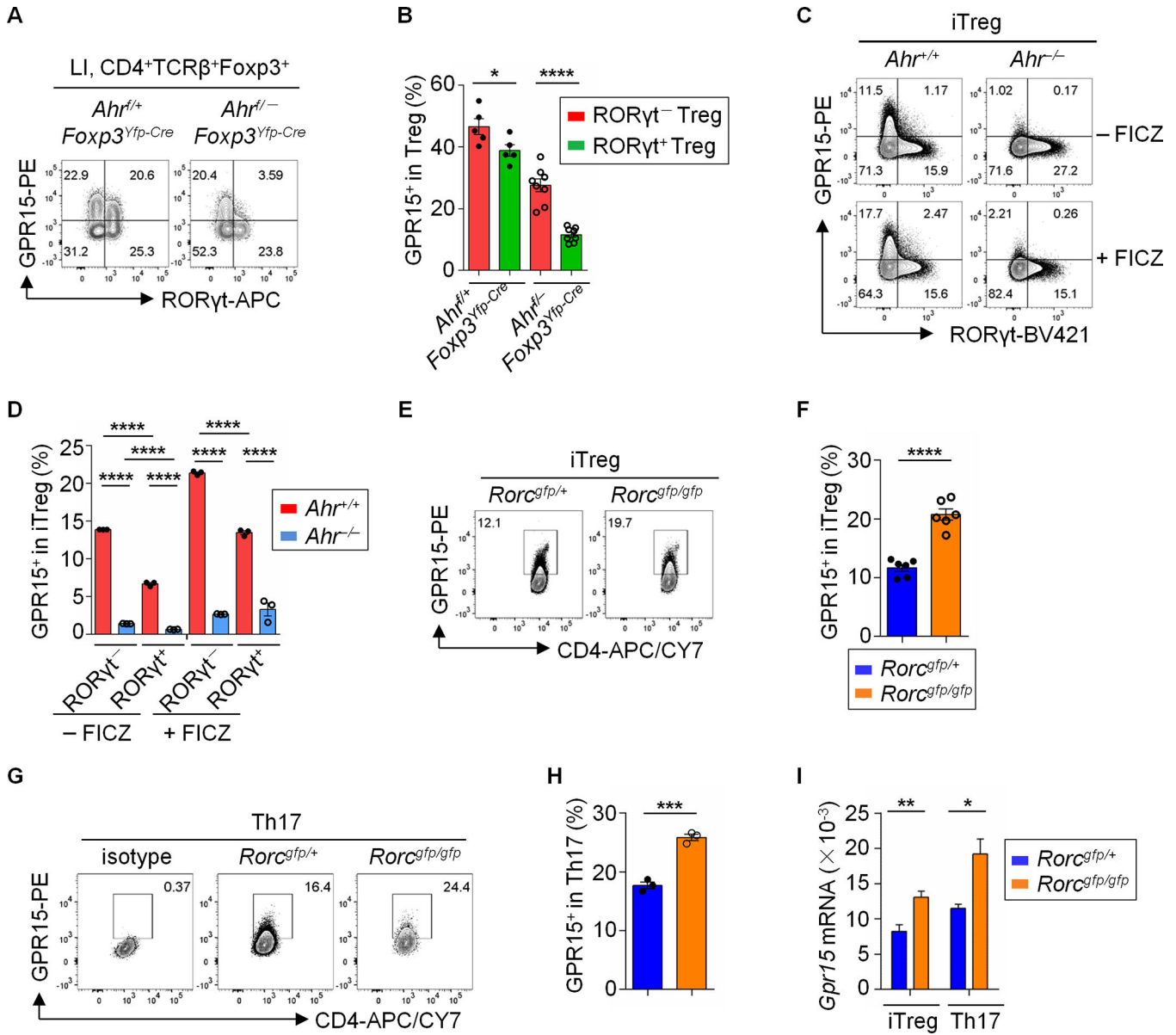
three independent experiments and are shown as mean ± SEM (n = 4). Ahr enrichment at *Cyp1a1* and *Il12b* locus were used as positive and negative controls respectively for Ahr ChIP assay. (**F**) Flow cytometry analysis of GPR15 expression in iTregs transduced with retroviral constructs encoding MIG-Ahr, MIG-Y9A or control (MIG-EV). The cells were treated with FICZ at day 2. Data are representative of two independent experiments. (**G**) Percentages of the GPR15$^+$ proportion in iTregs from *Ahr$^{+/+}$* and *Ahr$^{-/-}$* littermate mice transduced with retroviral constructs encoding MIG-Ahr, MIG-Y9A or control (MIG-EV). Data are shown as mean ± SEM (n = 3–4).
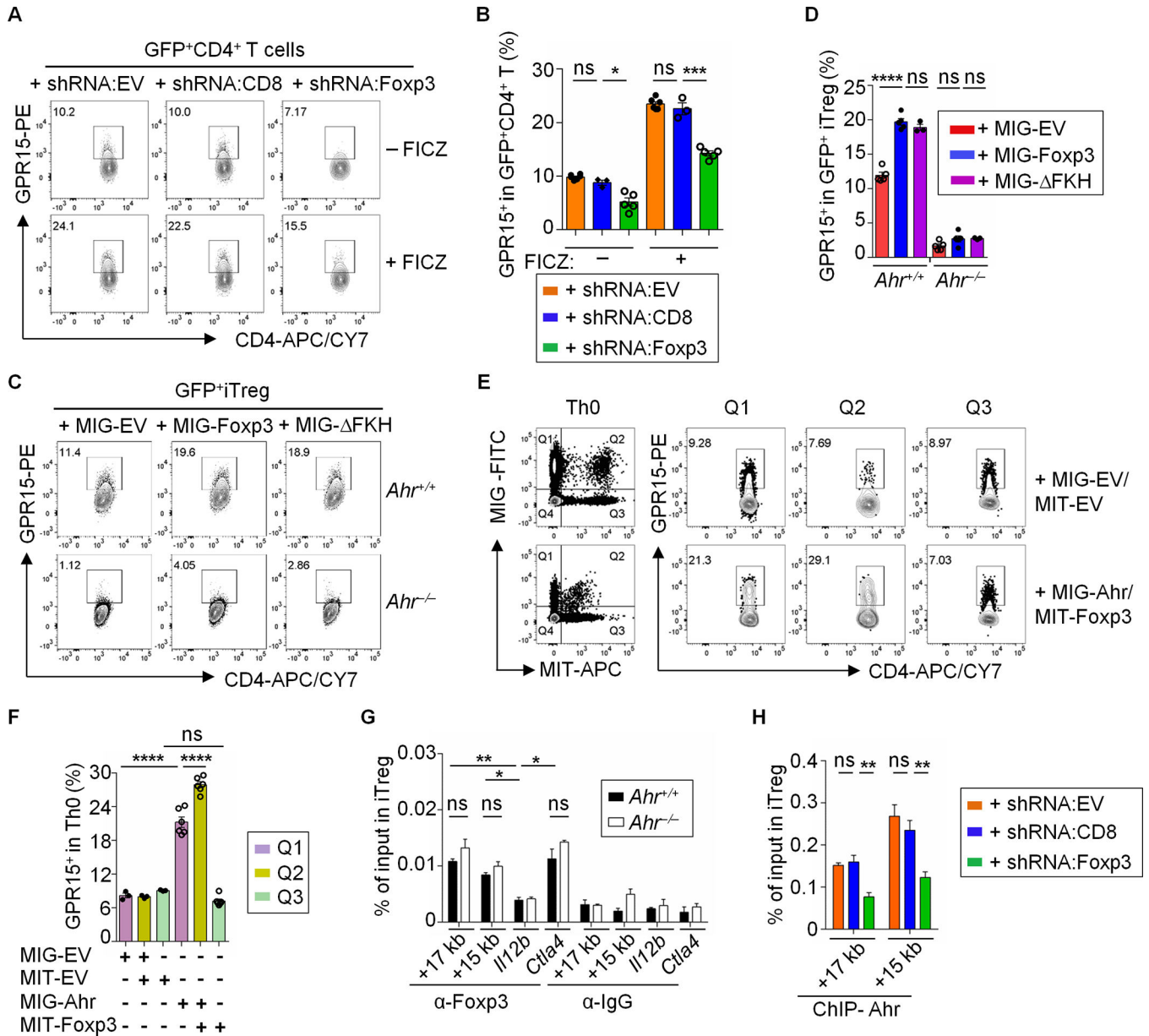
Fig. 3. Foxp3 cooperates with Ahr to positively regulate GPR15 expression.
(**A**) Flow cytometry analysis of GPR15 expression in CD4^{+} T cells under iTreg-polarizing conditions transduced with controls shRNA:EV (LMP) or shRNA:CD8, or shRNA:Foxp3 (LMP1066). Data are representative of three independent experiments. (**B**) Percentages of the GPR15^{+} proportion in CD4^{+} T cells transduced with shRNA:EV, shRNA:CD8 or shRNA:Foxp3. Data are shown as mean ± SEM (n = 3–6). (**C**) Flow cytometry analysis of GPR15 expression in iTregs transduced with control retroviral construct MSCV-IRES-GFP (MIG-EV), Foxp3-IRES-GFP (MIG-Foxp3) or Foxp3 FKH-IRES-GFP (MIG- FKH). Data are representative of three independent experiments. (**D**) Percentages of the GPR15^{+} proportion in iTregs transduced with MIG-EV, MIG-Foxp3 or MIG- FKH. Data are shown as mean ± SEM (n = 3–5). (**E**) Flow cytometry analysis of GPR15 expression by Th0 cells co-transduced with control retroviral constructs MIG-EV/MIT-EV or MIG-Ahr/MIT-Foxp3.

Data are representative of three independent experiments. (**F**) Percentages of the GPR15+ proportion in Th0 co-transduced with MIG-EV/MIT-EV or MIG-Ahr/MIT-Foxp3. Data are shown as mean ± SEM (n = 3–6). (**G**) Foxp3 ChIP assay of iTregs differentiated from naïve CD4+ T cells of $Ahr^{+/+}$ or $Ahr^{-/-}$ littermate mice. Enrichment of Foxp3 at the site 17 kb (+17 kb) or 15 kb (+15 kb) downstream of the transcription start site of $Gpr15$ was determined by real-time PCR. Data are representative of two independent experiments and are shown as mean ± SEM (n = 3). Foxp3 enrichment at the $Il12b$ or $Ctla4$ locus was used as negative or positive control, respectively. (**H**) Ahr ChIP assay of iTregs transduced with shRNA:EV, shRNA:CD8, or shRNA:Foxp3. Enrichment of Ahr at the site 17 kb (+17 kb) or 15 kb (+15 kb) downstream of the transcription start site of $Gpr15$ was determined by real-time PCR. Data are representative of two independent experiments and are shown as mean ± SEM (n = 3–6). Also see fig. S3.

A

LI, CD4+TCRβ+Foxp3+

*Ahr^f/+^*
*Foxp3^Yfp-Cre^*

*Ahr^f/−^*
*Foxp3^Yfp-Cre^*

GPR15-PE / RORγt-APC

22.9 | 20.6
31.2 | 25.3

20.4 | 3.59
52.3 | 23.8

B

GPR15+ in Treg (%)

- RORγt− Treg
- RORγt+ Treg

*Ahr^f/+^ Foxp3^Yfp-Cre^*
*Ahr^f/−^ Foxp3^Yfp-Cre^*

* / ****

C

iTreg

*Ahr^+/+^* | *Ahr^−/−^*

GPR15-PE / RORγt-BV421

− FICZ:
11.5 | 1.17
71.3 | 15.9

1.02 | 0.17
71.6 | 27.2

+ FICZ:
17.7 | 2.47
64.3 | 15.6

2.21 | 0.26
82.4 | 15.1

D

GPR15+ in iTreg (%)

- *Ahr^+/+^*
- *Ahr^−/−^*

RORγt− | RORγt+ | RORγt− | RORγt+
− FICZ | + FICZ

**** **** **** **** **** ****

E

iTreg

*Rorc^gfp/+^* | *Rorc^gfp/gfp^*

GPR15-PE / CD4-APC/CY7

12.1 | 19.7

F

GPR15+ in iTreg (%)

****

- *Rorc^gfp/+^*
- *Rorc^gfp/gfp^*

G

Th17

isotype | *Rorc^gfp/+^* | *Rorc^gfp/gfp^*

GPR15-PE / CD4-APC/CY7

0.37 | 16.4 | 24.4

H

GPR15+ in Th17 (%)

***

I

Gpr15 mRNA (×10^−3^)

- *Rorc^gfp/+^*
- *Rorc^gfp/gfp^*

iTreg | Th17

** | *

Fig. 4. RORγt negatively regulates GPR15 expression.

(**A**) Flow cytometry analysis of GPR15 and RORγt expression in Tregs from LI of the indicated littermate mice. Data are representative of three independent experiments. (**B**) Percentages of GPR15+ proportion in Tregs from LI of the indicated littermate mice. Data are shown as mean ± SEM (n = 5–8 mice per group). (**C**) Flow cytometry analysis of GPR15 and RORγt expression in iTregs (CD4+TCRβ+Foxp3+) from indicated littermate mice. Data are representative of three independent experiments. (**D**) Percentages of GPR15+ proportion in the sub-populations of iTregs from indicated mice. Data are shown as mean ± SEM (n = 3). (**E** and **G**) Flow cytometry analysis of GPR15 and CD4 expression in iTregs (CD4+TCRβ+Foxp3+) (**E**) or Th17 (CD4+TCRβ+Foxp3−IL-17+) (**G**) from indicated littermate mice. Data are representative of three independent experiments. (**F** and **H**) Percentages of GPR15+ proportion in iTregs (**F**) or Th17 (**H**) from indicated mice. Data are
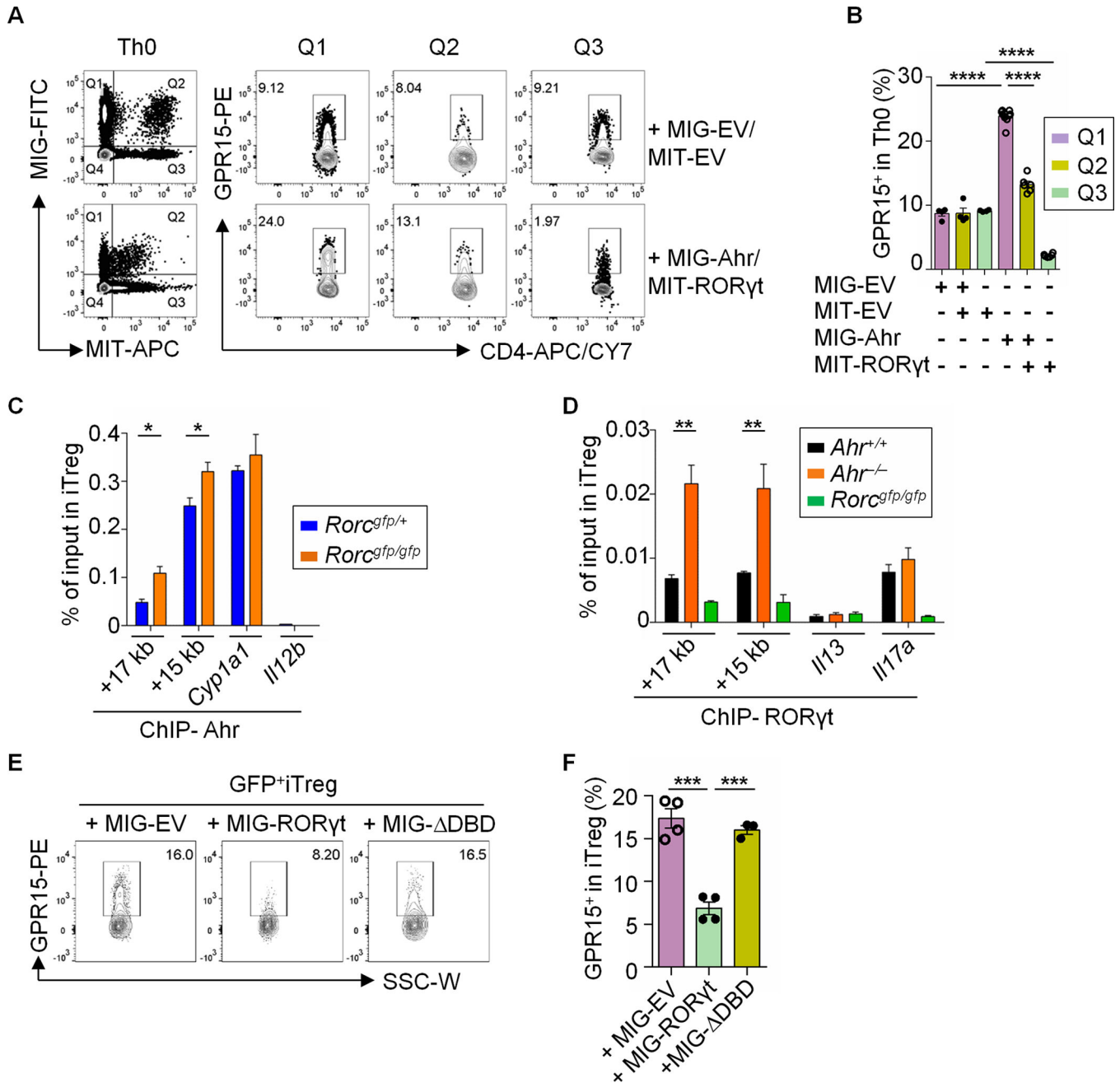
shown as mean ± SEM (n = 3–6). (**I**) Relative expression of *Gpr15* mRNA in iTregs and Th17 from indicated mice was analyzed by real-time RT-PCR. Data are representative of three independent experiments shown as mean ± SEM (n = 3).

Fig. 5. RORγt antagonizes Ahr for DNA binding at the *Gpr15* locus.
(**A**) Flow cytometry analysis of GPR15 expression by Th0 cells co-transduced with control retroviral constructs MIG-EV and MIT-EV or MIG-Ahr and MIT-RORγt. Data are representative of two independent experiments. (**B**) Percentages of the GPR15+ proportion by Th0 cells co-transduced with MIG-EV and MIT-EV or MIG-Ahr and MIT-RORγt. Data are shown as mean ± SEM (n = 4–6). (**C**) ChIP assay of iTregs from *Rorc*gfp/+ or *Rorc*gfp/gfp littermate mice. Enrichment of Ahr at the site 17 kb (+17 kb) or 15 kb (+15 kb) downstream of the transcription start site of *Gpr15* was determined by real-time PCR. Data are representative of two independent experiments and are shown as mean ± SEM (n = 3). Ahr

enrichment at *Cyp1a1* and *Il12b* locus were used as positive and negative controls respectively. (**D**) ChIP assay of iTregs from $Ahr^{+/+}$ or $Ahr^{-/-}$ littermate mice. Enrichment of RORγt at the site 17 kb (+17 kb) or 15 kb (+15 kb) downstream of the transcription start site of *Gpr15* was determined by real-time PCR. Data are representative of two independent experiments and are shown as mean ± SEM (n = 4). RORγt enrichment at the *Il13* or *Il17a* locus was used as negative or positive control, respectively. (**E**) Flow cytometry analysis of GPR15 expression in iTregs transduced with MIG-EV, MIG-RORγt or MIG- DBD. Data are representative of three independent experiments. (**F**) Percentages of the GPR15$^+$ proportion in iTregs from $Rorc^{gfp/gfp}$ mice transduced with MIG-EV, MIG-RORγt or MIG- DBD. Data are shown as mean ± SEM (n = 3–4). Also see fig. S4.
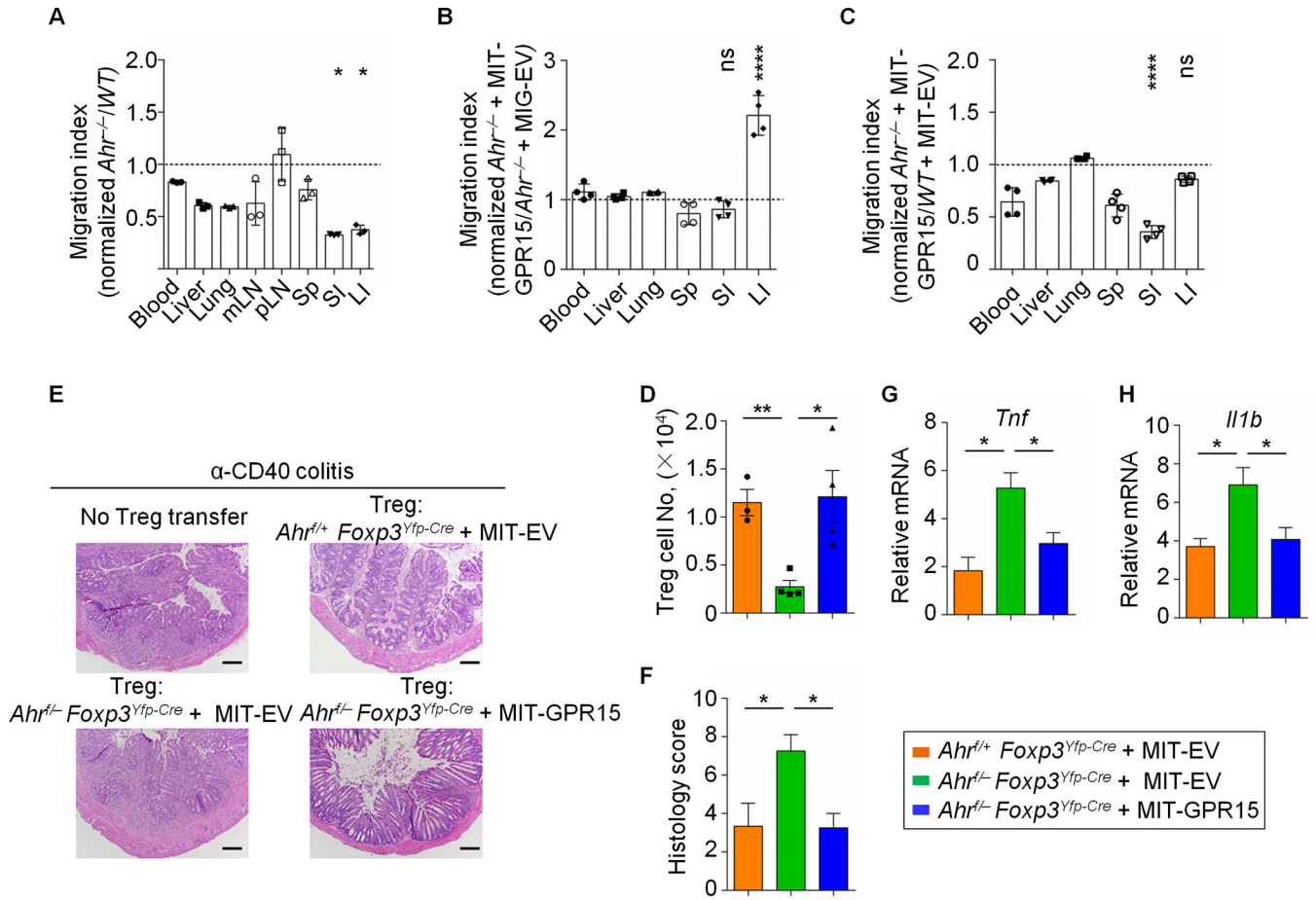
Fig. 6. Ahr promotes gut homing of Tregs by regulating GPR15.

(**A**) Migration index of donor cells (iTregs) from $Ahr^{+/+}$ (*CD45.1/CD45.1*) and $Ahr^{-/-}$ (*CD45.2/CD45.2*) mice in different organs of recipients 10 h post transfer. The migration index was calculated using the following formula: migration index = (ratio of CD45.1$^-$/ CD45.1$^+$ Tregs in post-transfer)/(ratio of CD45.1$^-$/CD45.1$^+$ Tregs in input). Data are representative of two independent experiments and shown as mean ± SEM (n = 3 mice per group). One-way ANOVA with Dunnett's multiple comparisons test was used to compare large intestine or small intestine to the other organs. (**B**) GPR15 transduction rescued the colon homing deficiency of Tregs from $Ahr^{-/-}$ mice. Migration index of MIT-GPR15- and MIG-EV- transduced iTregs from $Ahr^{-/-}$ mice in different organs 10 h post transfer. The migration index was calculated using the following formula: migration index = (ratio of $Ahr^{-/-}$ transduced with MIT-GPR15/ $Ahr^{-/-}$ transduced with MIG-EV Tregs in post-transfer)/ (ratio of $Ahr^{-/-}$ transduced with MIT-GPR15/ $Ahr^{-/-}$ transduced with MIG-EV Tregs in input). Data are representative of two independent experiments and shown as mean ± SEM (n = 4 mice per group). One-way ANOVA with Dunnett's multiple comparisons test was used to compare large intestine or small intestine to the other organs. (**C**) Migration index of MIT-GPR15-transduced iTregs from $Ahr^{-/-}$ (*CD45.2/CD45.2*) and MIT-EV-transduced iTregs from $Ahr^{+/+}$ (*CD45.1/CD45.1*) mice in different organs 10 h post transfer. The migration index was calculated using the following formula: migration index = (ratio of Ahr

$^{-/-}$ transduced with MIT-GPR15/ *Ahr*$^{-/-}$ transduced with MIT-EV Tregs in post-transfer)/ (ratio of *Ahr*$^{-/-}$ transduced with MIT-GPR15/ *Ahr*$^{+/+}$ transduced with MIT-EV Tregs in input). Data are representative of two independent experiments and shown as mean ± SEM (n = 4 mice per group). One-way ANOVA with Dunnett's multiple comparisons test was used to compare large intestine or small intestine to the other organs. (**D**–**H**) Adoptive transfer of Ahr-deficient iTregs transduced with MIT-GPR15 promoted their homing to the large intestine and suppressed gut inflammation in the α-CD40 colitis model. (**D**) Absolute Treg cell numbers in the colon of recipient *Rag1*$^{-/-}$ mice transferred with MIT-GPR15- or MIT-EV- transduced iTregs from *Ahr*$^{f/+}$ *Foxp3*$^{Yfp-Cre}$ or *Ahr*$^{f/-}$ *Foxp3*$^{Yfp-Cre}$ mice (n = 3–4 mice per group). (**E** and **F**) Hematoxylin/Eosin (H&E) histology sections of representative colon (10×; scar bar: 150 μm) (**E**) and clinical histology score (**F**). (**G** and **H**) Realtime RT-PCR of proinflammatory cytokine expression (i.e., *Tnf* and *Il1b*). Data are representative of two independent experiments and shown as mean ± SEM (n = 3–4 mice per group). Also see fig. S5.
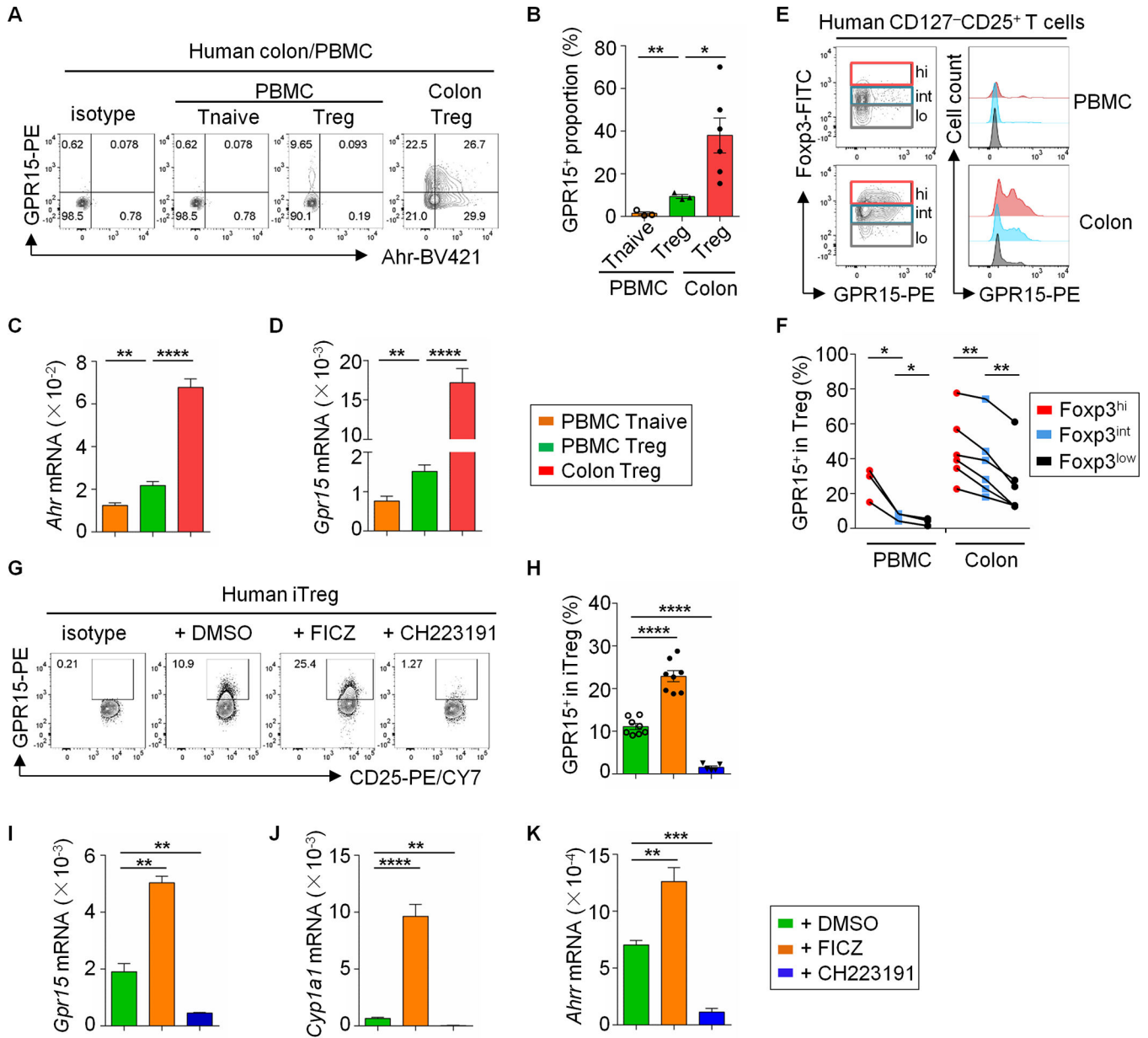
Fig. 7. Ahr signaling promotes GPR15 expression in human Tregs.
(**A**) Flow cytometry analysis of GPR15 and Ahr expression in human PBMC and colonic Tregs (CD3$^+$CD4$^+$CD45RA$^-$CD45RO$^+$CD127$^-$CD25$^+$Foxp3$^+$). Data are representative of three independent experiments. (**B**) Percentages of GPR15$^+$ proportion in Tregs from human PBMC and colonic LPLs. Data are shown as mean ± SEM (n = 3–6). (**C** and **D**) *Ahr* mRNA (**C**) had a positive correlation with that of *Gpr15* (**D**) in human Tregs. Data are shown as mean ± SEM (n = 4–6). (**E**) The expression of GPR15 by each CD127$^-$CD25$^+$ T cell subset defined by different levels of Foxp3 expression, depicted in color (i.e., red, blue and grey; left column) was analyzed by flow cytometry (right column). Data are representative of three independent experiments. (**F**) Percentages of the GPR15$^+$ proportion in each CD127$^-$CD25$^+$ T cell subset defined by different levels of Foxp3 expression from PBMC and human colon.

The symbols connected with a line represent data from the same individual donors (n = 3–6). The statistical analysis was performed with paired Student's t test. (**G**) Flow cytometry analysis of GPR15 and CD25 expression in iTregs (CD4$^+$CD45RA$^-$CD45RO$^+$CD127$^-$ CD25$^+$Foxp3$^+$) from sorted naïve CD4$^+$ T cells (CD3$^+$CD4$^+$CD45RA$^+$CD25$^-$) of PBMC, with the addition of DMSO, FICZ or CH223191. Data are representative of three independent experiments. (**H**) Percentages of GPR15$^+$ proportion in sub-population of iTregs with indicated treatment. Data are shown as mean ± SEM (n = 5–8). (**I–K**) The mRNA level of *Gpr15* and other Ahr target genes (*Cyp1a1* and *Ahrr*) was enhanced by FICZ addition while abolished by CH223191 treatment. Data are representative of three independent experiments and shown as mean ± SEM (n = 5). See also fig. S6.